RSC Publishing Faraday Discussions

FDPHOTOC15: Photoinduced electron transfer (PET) versus excimer formation in supramolecular p/n-heterojunctions of perylene bisimide dyes and implications for organic photovoltaics

Journal:	*Faraday Discussions*
Manuscript ID:	FD-ART-05-2015-000052.R1
Article Type:	Paper
Date Submitted by the Author:	26-Jun-2015

Complete List of Authors:	Nowak-Krol, Agnieszka; Universität Würzburg, Institute of Organic Chemistry Fimmel, Benjamin; Universität Würzburg, Institute of Organic Chemistry Son, Minjung; Yonsei University, Department of Chemistry Kim, Dongho; Yonsei University, Würthner, Frank; Universität Würzburg, Institute of Organic Chemistry

Photoinduced electron transfer (PET) *versus* excimer formation in supramolecular p/n-heterojunctions of perylene bisimide dyes and implications for organic photovoltaics

Agnieszka Nowak-Król,[a] Benjamin Fimmel,[a] Minjung Son,[b] Dongho Kim,*[,b] and Frank Würthner*[,a]

DOI: 10.1039/b000000x [DO NOT ALTER/DELETE THIS TEXT]

Foldamer systems comprised of two perylene bisimide (PBI) dyes attached to the conjugated backbones of 1,2-bis(phenylethynyl)benzene and phenylethynyl-bis(phenylene)indane, respectively, were synthesized and investigated with regard to their solvent-dependent properties. UV/Vis absorption and steady-state fluorescence spectra show that both foldamers prevail in a folded H-aggregated state consisting of π–π-stacked PBIs in THF and in more random conformations with weaker excitonic coupling between the PBIs in chloroform. Time-resolved fluorescence spectroscopy and transient absorption spectroscopy reveal entirely different relaxation pathways for the photoexcited molecules in the given solvents, *i.e.* photoinduced electron transfer leading to charge separated states for the open conformations (in chloroform) and relaxation into excimer states with red-shifted emission for the stacked conformations (in THF). Supported by redox data from cyclic voltammetry and Rehm-Weller analysis we could relate the processes occurring in these solution-phase model systems to the elementary processes in organic solar cells. Accordingly, only if relaxation pathways such as excimer formation are strictly avoided in molecular semiconductor materials, excitons may diffuse over larger distances to the heterojunction interface and produce photocurrent *via* the formation of electron/hole pairs by photoinduced electron transfer.

Introduction

The beneficial feature that molecular materials can be tailored with regard to their functional properties, *e.g.* absorption, ionization potential, and electron affinity, has been emphasized for many applications[1] despite the fact that mostly inorganic materials continue to dominate the latter, at least in the areas of electronics and photonics. The reason might be that whilst molecular properties can indeed be tailored, significant changes occur in the solid state due to the impact of supramolecular packing[2,3] and in particular disorder,[4] giving rise to undesired and hardly predictable changes of the desired properties. This general problem is illustrated most convincingly by organic solar cells (OSCs) which require a heterojunction of a p- and n-type semiconductor to accomplish efficient exciton dissociation into free p- and n-type charge carriers.[5] At first glance, this concept, as originally introduced by Tang,[6] is very simple and only requires proper adjustment of the redox levels of the two constituent organic semiconductor materials. As the field advances, however, researchers become aware that different orientations of the

molecules at the interfaces as well as the intermolecular contacts with their neighbour molecules have a crucial impact on the device performance.[7] But it is very difficult to assign experimentally the mutual arrangement of the molecules at the interface and to distinguish between the detrimental effects arising from a less suitable ordered arrangement (*e.g.* co-facial stacking *vs.* edge-on arrangement of the p- and n-type semiconductor molecules at the interface, *cf.* Fig. 1a,b) and from disordered arrangements that are known to create trap sites.[4] Likewise, it is not trivial to distinguish detrimental effects related to the interfacial organization of p- and n-semiconductor molecules from other problems such as charge carrier extraction within either of the two semiconductor materials which have to transport the holes and the electrons to the respective electrodes.[8]

In contrast to the complexity of bulk heterojunction (BHJ) OSC materials, photophysical properties in molecular dyads composed of electron donor (D) and acceptor (A) molecules are much easier to access by photophysical studies.[9-12] However, for typical D-A dyad systems, packing effects arising from polarization, excitonic coupling, *etc.* on the electronic properties of the constituent functional building blocks are not included at all. To overcome this deficiency, several groups have started to prepare supramolecular p/n-heterojunctions and to study their photophysical properties.[13-15]

In most of these studies the supramolecular systems were obtained by self-assembly, leading to larger structures that are not well-defined with regard to the exact packing arrangements and the size of the aggregates. In contrast, our recent research interest has been dedicated to small model systems composed of electron-rich oligo-phenylene ethynylene backbones (p-type semiconductor molecules) with electron-poor perylene bisimides (PBIs; n-type semiconductor molecules) appended to them, whose supramolecular arrangement can be modulated between more random and more folded conformations by the chosen solvent.[16-18] Accordingly, photophysical properties can be compared for the same molecules in two states of different order, which is analogous to the situation in more crystalline and more amorphous bulk heterojunction OSC materials (Fig. 1). PBIs are indeed particularly useful n-type semiconductors for such studies because their properties are known to depend very sensitively on the packing arrangements.[19,20] This might also be the reason why only few high performance OSCs are known based on PBI based acceptor components[21,22] in contrast to fullerenes which in general perform well. We envisage that fundamental studies like the one provided here may help to understand the problems encountered by packing and disorders in PBI-based materials and to derive guidelines for the design of PBI dyes for OSCs with improved performance.

Towards this goal, herein we investigate two PBI folda-dimers **F2** and **F2S** with stationary and time-resolved absorption and fluorescence spectroscopies as well as cyclic and square wave voltammetry, and relate the electrochemical and photophysical results to processes that may take place in OSCs.

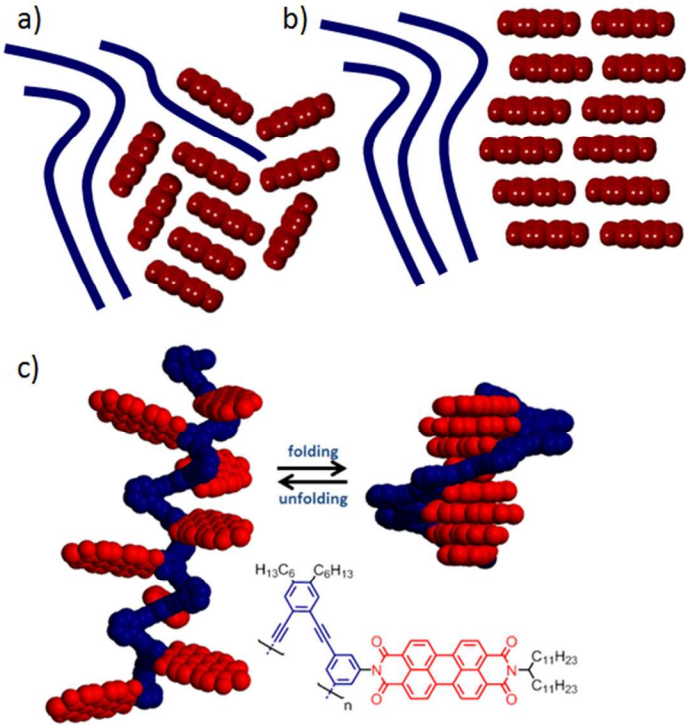

Fig. 1 Schematic representation of a) a more disordered and b) a more ordered p/n-heterojunction material composed of a p-type electron-donating semiconducting polymer (blue) and electron-accepting n-type semiconducting PBI molecules (red) and c) folding-dependent equilibrium between more disordered (left) and more ordered (right) supramolecular p/n-heterojunction composed of an electron-rich semiconducting backbone and appended electron-accepting PBIs.

Experimental Section

General: All reagents were purchased from commercial sources and used as received without further purification, unless otherwise stated. 1,4-Dioxane was kept for several days over KOH, then refluxed with sodium and stored over molecular sieves 3 and 4 Å. The synthesis and characterization of monomeric PBI reference molecules *N*-(3-iodophenyl)-*N*'-(1-undecyldodecyl)perylene-3,4:9,10-tetracarboxylic acid bisimide (**M1**)[17] and *N*-(4,5-di-*n*-hexyl-1,2-(phenylethynylene)benzene-functionalized *N*'-(1-undecyldodecyl)perylene-3,4:9,10-tetracarboxylic acid bisimide (**M2**),[17] folda-dimer **F2**,[17] and 4,5-di-*n*-hexyl-1,2-(phenylethynylene)-benzene backbone (**B**)[18] were reported recently. Column chromatography was performed on silica (silica gel, 230-400 mesh). Recycling gel permeation chromatography (GPC) was performed on a Shimadzu GPC system (LC-20AD prominence pump; SPD-MA20A prominence diode array detector) equipped with two preparative columns (JAIGEL 1H+2H) with $CHCl_3$ as eluent at a flow rate of 3.5 mL min^{-1} and a pressure of 20 MPa. ^1H, ^{13}C, and DEPT-135 NMR spectra were recorded on Bruker Avance 400 or Bruker DMX 600 spectrometers and calibrated to the residual solvent signals. High resolution mass spectra (ESI) were recorded on an ESI micrOTOF Focus spectrometer from Bruker Daltonics.

Cyclic voltammetry (CV): The CV measurements were performed on a standard, commercial electrochemical analyzer (EC epsilon; BAS Instruments, UK) in a three electrode single-compartment cell in an argon atmosphere. Dichloromethane (HPLC grade) was dried over calcium hydride in an argon atmosphere and degassed prior to use. The supporting electrolyte NBu_4PF_6 was synthesized according to literature,[23] recrystallized from ethanol/water, and dried in high vacuum. The measurements were carried out under exclusion of air and moisture at a concentration of approximately $2.5 \cdot 10^{-4}$ M with ferrocene as an internal standard for the calibration of the potential. Working electrode: Pt disc; reference electrode: Ag/AgCl; auxiliary electrode: Pt wire.

Steady-state UV/Vis absorption and fluorescence spectroscopy: All spectroscopic measurements were conducted with spectroscopic grade solvents (Uvasol®) from Merck (Hohenbrunn, Germany) by using conventional quartz cells (light path 1 cm). UV/Vis spectra were recorded on Perkin-Elmer UV/Vis spectrometers Lambda 35 or Lambda 950. Steady-state fluorescence emission spectra were recorded with a PTI QM-4/2003 spectrometer. Polarizers in the specified set-up applying magic angle conditions (54.7°) or vertical orientation were used. The fluorescence quantum yields were determined by optical dilution method ($OD_{max} < 0.05$) and were determined as the average value for three to five different excitation wavelengths using *N*,*N'*-bis-(2,6-diisopropylphenyl)perylene 3,4:9,10-tetracarboxylic acid bisimide (Φ_{fl} ($CHCl_3$) = 1.00)[24] or pyrene (Φ_{fl} (cyclohexane) = 0.32)[25] as reference compounds.

Time-resolved fluorescence spectroscopy: Time-resolved fluorescence decays were obtained by using a time-correlated single photon counting (TCSPC) technique. A mode-locked Ti:sapphire oscillator (MaiTai-BB, SpectraPhysics) was used as the excitation light source, which provides a FWHM (full width at half maximum) of 80 fs with a high repetition rate of 80 MHz. In order to minimize artefacts such as thermal lensing and accumulation effect, the repetition rate was reduced down to 800 kHz using a home-made acousto-optic pulse selector. The picked fundamental pulses were frequency-doubled by a BBO nonlinear crystal (Eksma) of 1 mm thickness. The fluorescence was collected by a microchannel plate photomultiplier (MCP-PMT, R3809U-51, Hamamatsu) with a thermoelectric cooler (C4878, Hamamatsu). Time-resolved fluorescence signals were calculated by a TCSPC board (SPC-130, Becker & Hickel GmbH). The overall instrumental response function (IRF) was determined to be less than 30 ps (FWHM) in all spectral regions. The polarization of the photoexcitation pulses was set to be vertical to the laboratory frame by a half-wave retarder and a Glan laser polarizer, and sheet polarizers were used in the fluorescence collection path at magic angle (54.7°) to obtain polarization-independent population decays when measuring the fluorescence decay profiles.

Transient absorption spectroscopy (TA): The femtosecond time-resolved transient absorption (fs-TA) spectrometer consists of an optical parametric amplifier (OPA; Palitra, Quantronix) pumped by a Ti:sapphire regenerative amplifier system (Integra-C, Quantronix) operating at 1 kHz repetition rate and an optical detection system. The generated OPA pulses have a pulse width of ~100 fs and an average power of 1 mW in the range of 280-2700 nm, which are used as pump pulses. White

light continuum (WLC) probe pulses were generated using a sapphire window (3 mm thick) by focusing a small portion of the fundamental 800 nm pulses, which was picked off by a quartz plate before entering the OPA. The time delay between pump and probe beams was carefully controlled by making the pump beam travel along a variable optical delay (ILS250, Newport). Intensities of the spectrally dispersed WLC probe pulses were monitored by a High Speed Spectrometer (Ultrafast Systems) for both visible and near-infrared measurements. To obtain the time-resolved transient absorption difference signal (ΔA) at a specific time, the pump pulses were chopped at 500 Hz and absorption spectra intensities were saved alternately with or without pump pulse. Typically, 4000 pulses excite the samples to obtain the fs-TA spectra at each delay time. The polarization angle between pump and probe beam was set at the magic angle (54.7°) using a Glan laser polarizer with a half-wave retarder in order to prevent polarization-dependent signals. Cross-correlation FWHM in pump-probe experiments was less than 200 fs and chirp of WLC probe pulses was measured to be 800 fs in the 400-800 nm region. To minimize chirp, all reflection optics in the probe beam path and a quartz cell of 2 mm path length were used. After fs-TA experiments, the absorption spectra of all compounds were carefully examined to detect if there were artefacts due to degradation and photo-oxidation of samples. The three-dimensional data sets of ΔA versus time and wavelength were subjected to singular value decomposition and global fitting to obtain the kinetic time constants and their associated spectra using Surface Xplorer software (Ultrafast Systems).

Synthesis of singly-cyclized PBI folda-dimer F2S.

A dried Schlenk tube was charged with $Co_2(CO)_8$ (7 mg, 0.020 mmol). The solid was dried under reduced pressure and the vessel was purged with argon. PBI foldamer **F2** (14 mg, 7.5 µmol) was dried under vacuum, dissolved in anhydrous toluene (7.2 mL) and transferred to the Schlenk tube. Then dioxane (1.8 mL) was added and the mixture was heated to 100 °C. To a dried round-bottomed flask containing another portion of $Co_2(CO)_8$ (7 mg, 0.020 mmol) anhydrous toluene (10 mL) was added, followed by 1,6-heptadiyne (23 µL, 0.20 mmol) and the solution was added dropwise *via* a syringe pump over 17 h. Then the stirring at 100 °C was continued for 6 h. Afterwards, the solvents were removed *in vacuo* and the crude product was purified by column chromatography (silica, CH_2Cl_2, then CH_2Cl_2 + 0.5% MeOH) and singly-cyclized product **F2S** was separated from small amounts of doubly-cyclized product by recycling GPC ($CHCl_3$) to afford pure folda-dimer **F2S** (5 mg, 34%). UV/Vis λ_{max}($CHCl_3$, c = $6.3 \cdot 10^{-6}$ M)/nm 527 (ε/dm^3 mol^{-1} cm^{-1} 93 000), 491 (80 000), 461 (31 400), 369 (6 200), 261 (72 500). UV/Vis λ_{max}(THF, c = $5.7 \cdot 10^{-6}$ M)/nm 526 (ε/dm^3 mol^{-1} cm^{-1} 53 500), 491 (76 900), 462 (33 000), 370 (5 600). ^{1}H NMR (400 MHz; CD_2Cl_2; 25 °C) δ 8.65-8.29 (8 H, m, ArH_{pery}), 8.28-7.95 (8 H, m, ArH_{pery}), 7.79 (1 H, s, ArH), 7.63 (1 H, s, ArH), 7.45 (1 H, s, ArH), 7.38-7.31 (3 H, m, ArH), 7.29 (1 H, s, ArH), 7.26 (1 H, s, ArH), 7.19-7.09 (2 H, m, ArH), 7.03 (1 H, dm, J = 8.1 Hz, ArH), 6.99 (1 H, dm, J = 8.1, ArH), 5.24-5.07 (1 H, m, NCH), 5.07-4.90 (1 H, m, NCH), 3.13-2.89 (4 H, m, CH_{2cycl}), 2.82-2.56 (4 H, m, CCH_2), 2.40-2.16 (4 H, m, $CH_2(CH_2)_2$), 2.15-2.08 (2 H, m, CH_{2cycl}), 2.06-1.77 (4 H, m, $CH_2(CH_2)_2$), 1.73-1.60 (4 H, m, CH_2), 1.49-1.00 (84 H, m, CH_2), 0.98-0.71 (18 H, m, CH_3). ^{13}C NMR (151 MHz; $CDCl_3$; 25 °C) δ 163.3, 163.2, 163.0, 144.00, 143.8, 143.3, 142.2, 141.2, 139.3, 138.8, 137.8, 135.0, 134.8, 134.5, 134.4, 133.9, 132.7 ($C_{Ar}H$), 132.4 ($C_{Ar}H$), 132.0 ($C_{Ar}H$), 131.7 ($C_{Ar}H$), 131.6 ($C_{Ar}H$), 131.5

($C_{Ar}H$), 130.9 ($C_{Ar}H$), 130.8 ($C_{Ar}H$), 130.2, 129.9 ($C_{Ar}H$), 129.9 ($C_{Ar}H$), 129.7, 129.5, 129.31, 129.25, 128.8 ($C_{Ar}H$), 128.2 ($C_{Ar}H$), 127.6 ($C_{Ar}H$), 126.8 ($C_{Ar}H$), 126.26, 126.24 ($C_{Ar}H$), 126.08, 126.06, 125.97 ($C_{Ar}H$), 125.3, 123.6, 123.0 ($C_{Ar}H$), 120.0, 90.8 (C_{triple}), 89.9 (C_{triple}), 55.2 (NCH), 55.1 (NCH), 37.7 (CH_2), 37.61 (CH_2), 37.56 (CH_2), 37.3 (CH_2), 33.3 (CH_2), 32.93 (CH_2), 32.85 (CH_2), 32.83 (CH_2), 32.7 (CH_2), 32.6 (CH_2), 32.5 (CH_2), 32.4 (CH_2), 32.1 (CH_2), 31.96 (CH_2), 31.93 (CH_2), 31.90 (CH_2), 31.28 (CH_2), 31.24 (CH_2), 31.15 (CH_2), 31.09 (CH_2), 30.3 (CH_2), 30.2 (CH_2), 29.9 (CH_2), 29.81 (CH_2), 29.80 (CH_2), 29.76 (CH_2), 29.72 (CH_2), 29.65 (CH_2), 29.60 (CH_2), 29.50 (CH_2), 29.48 (CH_2), 29.39 (CH_2), 29.36 (CH_2), 29.27 (CH_2), 29.22 (CH_2), 28.1 (CH_2), 27.6 (CH_2), 27.43 (CH_2), 27.37 (CH_2), 27.3 (CH_2), 27.1 (CH_2), 25.70 (CH_2), 25.67 (CH_2), 24.9 (CH_2), 24.6 (CH_2), 22.93 (CH_2), 22.85 (CH_2), 22.82 (CH_2), 22.7 (CH_2), 20.0 (CH_3), 19.9 (CH_3), 14.6 (CH_3), 14.32 (CH_3), 14.28 (CH_3), 14.25 (CH_3). MS HR (ESI) *m/z* calcd for $C_{135}H_{155}N_4O_8$ $[M+H]^+$ 1960.1845, found 1960.1839.

Synthesis of singly-cyclized reference backbone BS.

A dried flask was charged with compound **B** (60 mg, 0.13 mmol), and $Co_2(CO)_8$ (128 mg, 0.37 mmol). The solids were dried under reduced pressure. Then the flask was purged with nitrogen, and anhydrous toluene (48 mL), followed by anhydrous 1,4-dioxane (16 mL) were added. The mixture was heated to 100 °C. In the second dried round-bottomed flask another portion of $Co_2(CO)_8$ (104 mg, 0.30 mmol) was placed and the solid was dried under vacuum. Then the flask was purged with nitrogen and anhydrous toluene (26 mL), followed by 1,6-heptadiyne (337 µL, 2.94 mmol) were added. The latter solution was added dropwise *via* a syringe pump over 17 h to the Schlenk flask containing a preheated solution of **B**. Then the stirring was continued for 5.5 h at 100 °C. Afterwards, the solvents were removed *in vacuo* and the crude product was purified by column chromatography (silica, *n*-hexane, then gradual change to *n*-hexane/CH_2Cl_2 97:3). All the fractions were purified another time by chromatography (silica, *n*-pentane, then gradual change to *n*-pentane/CH_2Cl_2 98:2) to obtain recovered compound **B** (32 mg, 53%) and singly-cyclized product **BS** (32 mg, 44%). UV/Vis λ_{max}($CHCl_3$, c = $1.30 \cdot 10^{-5}$ M)/nm 295 (ε/dm^3 mol^{-1} cm^{-1} 23 700), 280 (22 900), 313 (18 900). UV/Vis λ_{max}(CH_2Cl_2, c = $1.13 \cdot 10^{-5}$ M)/nm 295 (ε/dm^3 mol^{-1} cm^{-1} 25 100), 279 (24 400), 313 (19 500). ^{1}H NMR (400 MHz; CD_2Cl_2; 25 °C) δ 7.40 (1 H, s, ArH), 7.34-7.21 (7 H, m, ArH), 7.16-7.09 (5 H, m, ArH), 6.86 (1 H, s, ArH), 3.13-2.94 (4 H, m, CH_2), 2.62-2.52 (2 H, m, CH_{2cycl}), 2.53-2.40 (2 H, m, J = 7.2 Hz, CH_{2cycl}), 2.18 (2 H, p, J = 7.4 Hz, CH_{2cycl}), 1.65-1.49 (4 H, m, CH_2), 1.46 – 1.16 (12 H, m, CH_2), 0.99-0.83 (6 H, m, CH_3). ^{13}C NMR (101 MHz; CD_2Cl_2; 25 °C) δ 144.46, 143.37, 142.81, 142.39, 141.61, 140.07, 139.69, 137.91, 132.92 (CH), 132.72 (CH), 131.71 (CH), 130.31 (CH), 128.81 (CH), 128.36 (CH), 128.00 (CH), 127.46 (CH), 126.50 (CH), 126.35 (CH), 124.32, 120.29, 91.45 (C_{triple}), 90.60 (C_{triple}), 33.29 (CH_2), 33.25 (CH_2), 32.85 (CH_2), 32.71 (CH_2), 32.33 (CH_2), 32.30 (CH_2), 31.62 (CH_2), 31.47 (CH_2), 29.87 (CH_2), 29.66 (CH_2), 26.26 (CH_2), 23.21 (CH_2), 23.13 (CH_2), 14.46 (CH_3). MS HR (ESI) *m/z* calcd for $C_{41}H_{47}$ $[M+H]^+$ 539.3678, found 539.3672. Fluorescence (CH_2Cl_2): λ_{max} = 384 nm (λ_{ex} = 310 nm); Φ_{fl} = 0.58±0.008.

Additional spectral data for compound M1.

Fluorescence (CH_2Cl_2): λ_{max} = 534, 575, 626 nm (λ_{ex} = 480 nm); Φ_{fl} = 0.89±0.03.

Additional spectral data for compound B.
UV/Vis $\lambda_{max}(CHCl_3, c = 1.29 \cdot 10^{-5}$ M)/nm 281 (ε/dm^3 mol^{-1} cm^{-1} 67 900), 267 (40 300), 317 (22 400), 305 (22 300). UV/Vis $\lambda_{max}(CH_2Cl_2, c = 8.2 \cdot 10^{-6}$ M)/nm 281 (ε/dm^3 mol^{-1} cm^{-1} 71 500), 266 (42 500), 317 (23 400), 305 (23 100). ^{1}H NMR (400 MHz; $CDCl_3$; 25 °C) δ 7.62-7.52 (4 H, m, ArH), 7.39-7.29 (8 H, m, ArH), 2.64-2.56 (4 H, m, CH_2), 1.66-1.55 (4 H, m, CH_2CH_2), 1.45-1.27 (12 H, m, CH_2), 0.97-0.84 (6 H, m, CH_3).

Results

In this article we investigate the properties of relevance for OSCs, *i.e.* redox and optical properties of two perylene bisimide – phenylene ethynylene heterojunction model molecules **F2** and **F2S** in comparison to PBI monomers **M1** and **M2** as well as backbone molecules **B** and **BS** (Chart 1). In contrast to the more extended octamer depicted in Fig. 1,[16] folda-dimer molecules **F2** and **F2S** could be obtained as monodisperse compounds of high purity whilst they still exhibit the relevant features of solvent-dependent folding into π–π-stacked states.

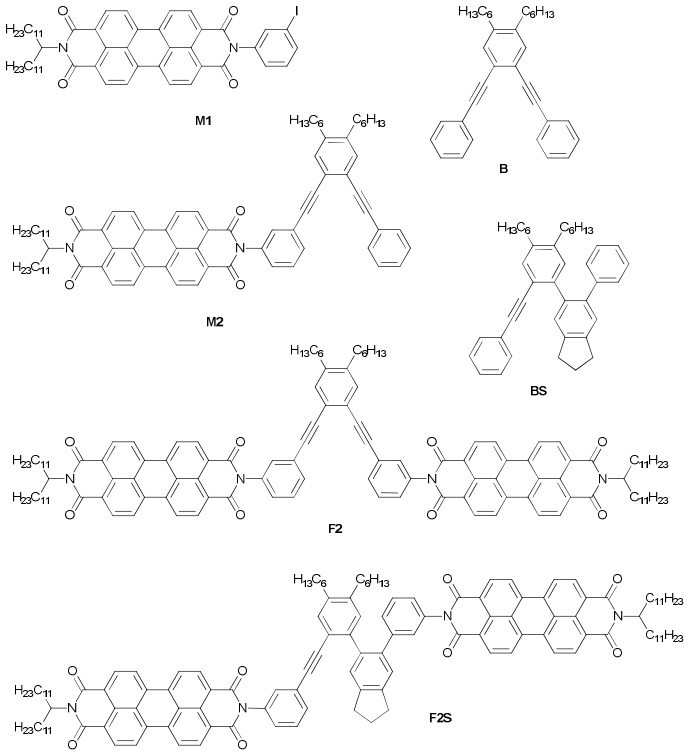

Chart 1 PBI-phenylene ethynylene heterojunction molecules **F2** and **F2S**, and monomeric PBI reference molecules **M1** and **M2** as well as backbone molecules **B** and **BS**.

Synthesis of new molecules

The energetically most favourable arrangement for PBI dyes in their aggregates consists of face-to-face stacks of rotationally displaced PBIs.[20] Accordingly, we may assume that such arrangements also prevail in composites with oligomeric or polymeric p-type semiconductors in non-crystalline BHJ OSC materials. Therefore, the formerly synthesized folda-dimer **F2**[17] appears to be a reasonable model system for an OSC p/n-heterojunction. In particular, because this molecule was shown to exhibit a solvent-dependent transition from a more random into a π-stacked folded conformation, photophysical studies may elucidate the different situations in OSCs related to packing arrangements. In our search for a second system, dicobalt-octacarbonyl-mediated cyclization between bis-PBI **F2** and 1,6-heptadiyne (**HD**, see Scheme 1) appeared to be an interesting possibility. An analogous transformation was applied in porphyrin chemistry by Fletcher and Therien[26] who described the formation of covalently bridged co-facial porphyrins *via* cycloaddition reaction between ethynylene-linked bis-porphyrins and 1,6-heptadiyne. Interestingly, in our study dicobalt-octacarbonyl-assisted cycloaddition of **F2** with **HD** afforded **F2S** in 34% yield along with unreacted starting material and only very small amount of doubly-cyclized product. Increasing the excess of $Co_2(CO)_8$ from *ca*. 5 to 10 eq., as well as 1,6-heptadiyne from *ca*. 27 to 63 eq. did not push the reaction towards larger amounts of **F2S** or doubly cyclized product, whereas the prolongation of the reaction provided only a complex mixture with a rather detrimental effect on the yield of **F2S**. Similar results were obtained for the PBI-free backbone **B** which could also be only converted to singly-cyclized **BS**. For this purpose a solution of **B** and $Co_2(CO)_8$ was treated with 1,6-heptadiyne and another portion of $Co_2(CO)_8$. The best yield for this reaction was obtained at higher dilution, affording exclusively singly-cyclized **BS**. Careful purification of the product by chromatography afforded pure **BS** as colourless oil in 44% yield, whereas 53% of the starting material could be recovered.

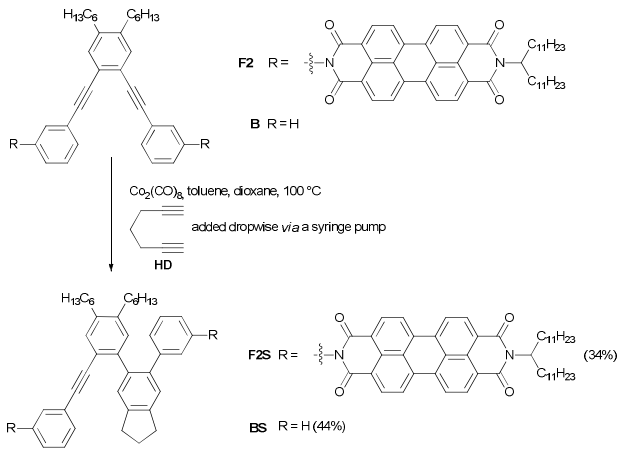

Scheme 1 Syntheses of singly-cyclized folda-dimer **F2S** and reference compound **BS**.

UV/Vis absorption and steady-state fluorescence spectroscopy

The UV/Vis absorption spectra of PBIs **M1**, **M2**, **F2**, and **F2S** were measured in $CHCl_3$ and THF because the solvation properties of these two solvents are

particularly suitable for inducing different degrees of π-stacking between the two PBI dyes (Fig. 2) according to our previous studies.[17] Thus, whilst very similar spectra are obtained for PBI monomer **M2** (and likewise for **M1**) in both solvents, a pronounced solvent effect is observed for **F2** and **F2S** (Fig. 3). This solvent effect is attributable to the different degrees of excitonic coupling between the two PBI dyes depending on the mutual interaction of their transition dipole moments.[27] The spectral features observed for **F2** and **F2S** in THF with reduced intensity at ~530 nm (0-0 vibronic transition of a PBI monomer) are indicative of closely π–π-stacked PBIs with a rotational displacement.[17,27] On the other hand, in $CHCl_3$, the spectra still resemble those of the monomers which can be taken as evidence for the presence of conformations with more distant PBIs with weaker excitonic coupling. Nevertheless, the ratio of the 0-0 to 0-1 electronic transition band intensities, which is typically taken as an index for the coupling strength,[28] is already changed from *ca.* 1.65 (for both monomers) to 1.28 (**F2**) and 1.16 (**F2S**) in $CHCl_3$, revealing that the interaction of the two PBIs is not negligible. In THF, the excitonic coupling is far more pronounced (Table 1), which suggests that the conformational space has been reduced by a folding process, leading to the prevalence of closely stacked PBIs. The smaller values for **F2S** in both solvents suggest that the energetic preference for stacked conformations is even higher for the singly-cyclized backbone. It is noteworthy that the concentration-dependent spectral changes are almost negligible, which clarifies that the folding process is not in competition with self-assembly processes of these bis-PBIs into larger aggregates.

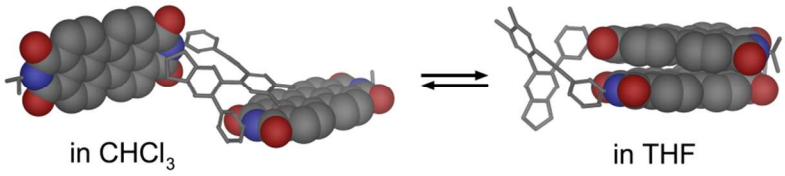

Fig. 2 Schematic representation of the solvent-dependent folding of folda-dimer **F2S**.

Table 1 Optical properties of dimers **F2**,[17] **F2S** and monomers **M1**,[17] **M2**[17] in $CHCl_3$ and THF.

Compd.	Solvent	$A_{0\text{-}0}/A_{0\text{-}1}$ [a]	λ_{em} [b] [nm]	Φ_{fl} [c] (%)
F2	$CHCl_3$	1.28	537, 580	28±2
	THF	0.81	533, 575, 615	16±2
F2S	$CHCl_3$	1.16	536, 579	18±2
	THF	0.70	531, 577, 617	18±2
M1	$CHCl_3$	1.66	532, 574	97±3
	THF	1.65	531, 571	97±6
M2	$CHCl_3$	1.64	537, 579	21±1
	THF	1.63	531, 571	36±5

[a] Ratio of the absorbance of 0-0 and 0-1 electronic transition bands. [b] Emission maxima. [c] Fluorescence quantum yields.

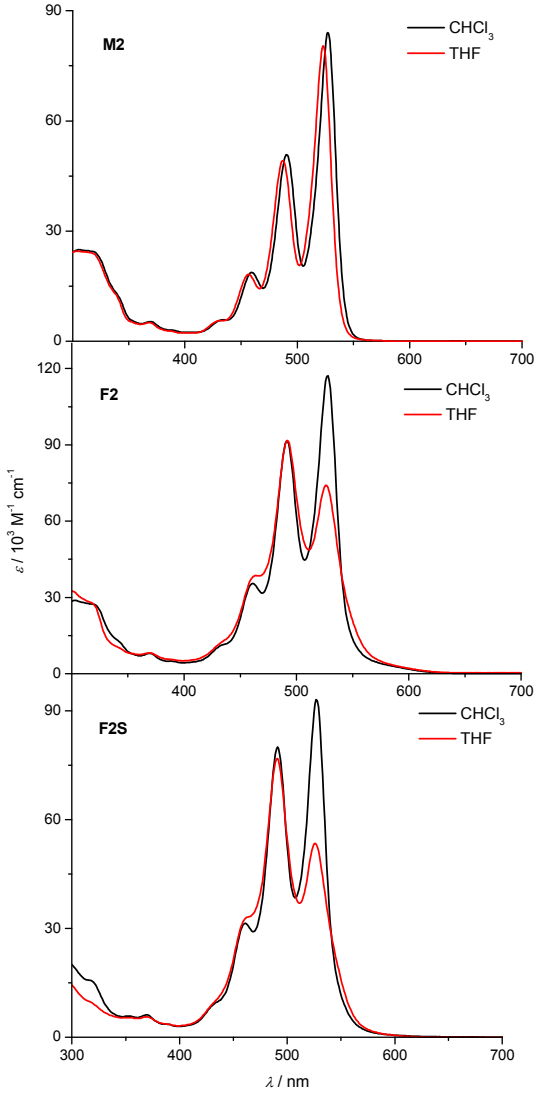

Fig. 3 UV/Vis absorption spectra of **M2** ($c = 1.06 \cdot 10^{-5}$ M, black line, and $c = 9.8 \cdot 10^{-6}$ M, red line), **F2** ($c = 7.2 \cdot 10^{-6}$ M, black line, and $c = 5.0 \cdot 10^{-6}$ M, red line), and **F2S** ($c = 6.3 \cdot 10^{-6}$ M, black line, and $c = 5.7 \cdot 10^{-6}$ M, red line) in $CHCl_3$ (black lines) and THF (red lines), respectively.

The steady-state fluorescence spectra corroborate the results from UV/Vis spectroscopy with regard to the conformational landscape of PBI folda-dimers **F2** and **F2S** (Fig. 4). To be more specific, the fluorescence spectra in chloroform are almost mirror images to the respective absorption spectra which indicates that there are little excitonic interactions among the two PBIs in the prevailing open random conformations. In contrast, a pronounced bathochromically displaced excimer band

shows up in THF, which can be attributed to strong interactions between the PBI molecules in the excited state, which necessitates close co-facial stacking arrangements. This effect is clearly more pronounced for **F2S** which suggests that the equilibrium between open random conformations and a face-to-face stacked conformation (Fig. 2) is more shifted towards the latter for this foldamer. Relaxation of co-facially stacked PBIs into excimer states is in general accompanied by a decrease of the fluorescence quantum yield which is also the case for folda-dimers **F2** and **F2S** (Table 1). Interestingly, whilst a decrease in the fluorescence quantum yield of **F2** is observed when changing from chloroform to THF (as expected due to the more favoured co-facially stacked conformation), equal values are observed for **F2S** in both solvents. As we will show later by transient absorption spectroscopy, this result can be explained by a second relaxation pathway *via* a photoinduced electron transfer (PET) process between the backbone and the PBI chromophore.

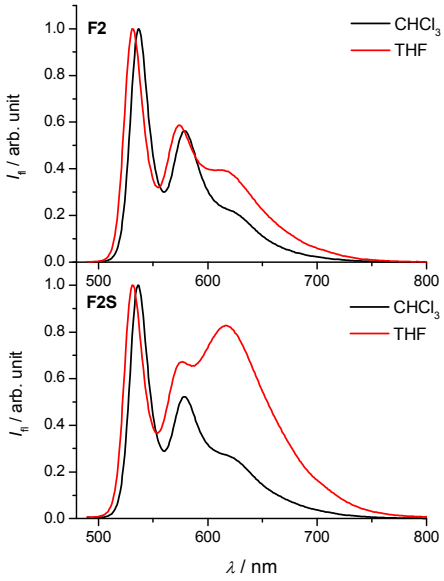

Fig. 4 Steady-state fluorescence spectra of **F2** (c = 2.5·10^{-6} M, black line, and c = 2.5·10^{-6} M, red line), and **F2S** (c = 2.5·10^{-6} M, black line, and c = 2.4·10^{-6} M, red line) in $CHCl_3$ and THF, respectively. For better comparison the intensities of all fluorescence bands were normalized to the 0-0 vibronic transitions.

Cyclic voltammetry

The ionization potential (IP) and the electron affinity (EA) of the p- and n-type semiconductors determine the energetics for a photoinduced charge separation process at a p/n-heterojunction interface and the magnitude of the open-circuit potential of the organic solar cell. The respective counterparts to these properties in the solid state are the oxidation and reduction potentials of donor and acceptor molecules within molecular dyads in solution.[29,30] Accordingly, we have determined

these values by cyclic voltammetry (CV) (Fig. 5) and collected the results in Table 2. It is noteworthy that the oxidation processes of both **B** and **BS** backbones were difficult to determine due to their irreversibility and the limited electrochemical window caused by oxidative decompositions of the solvent. Thus, only in acetonitrile we could resolve the oxidative peaks by CV for both backbones (see Fig. 5, left and Table 2). For **B**, on the other hand, the oxidation process could also be confirmed in dichloromethane at about +1.2 V *vs*. the ferrocene/ferrocenium redox couple by square wave voltammetry (Fig. S1). For the PBI reductions the situation was more favourable and two well-defined reductive waves could be measured for the monomeric PBIs **M1** and **M2**, as well as folda-dimer **F2**. For folda-dimer **F2S** clear differences are observed which suggest a different degree of PBI-PBI interactions during the stepwise loading of these molecules with up to four electrons. In depth investigations for a structurally related bis-PBI cyclophane have been performed recently[31] but are beyond the scope of the current study.

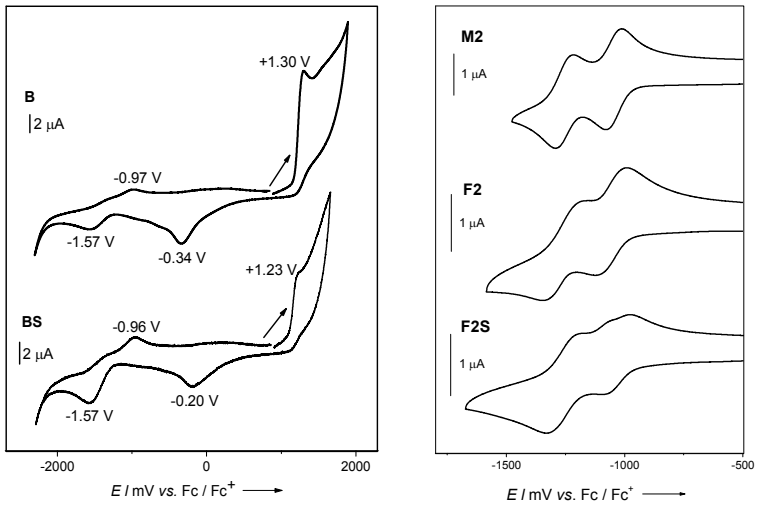

Fig. 5 Left: Cyclic voltammograms of **B** and **BS** in MeCN solutions of Bu_4NPF_6 initiated in the forward (positive-going) scan direction (marked by an arrow) at a scan rate of 100 mV s^{-1}. Right: Cyclic voltammograms of **M1**, **F2**, and **F2S** in CH_2Cl_2 solutions of Bu_4NPF_6 at a scan rate of 100 mV s^{-1}. The measurements were calibrated with an internal standard (ferrocene/ferrocenium).

Table 2 Half-wave reduction and oxidation potentials of investigated molecules.[a]

Compd.	$E_{1/2}$ (Red2) [V]	$E_{1/2}$ (Red1) [V]	$E_{1/2}$ (Ox) [V]
F2	–1.25	–1.06	–
F2S	–1.26	–1.04	–
M1	–1.27	–1.04	–
M2	–1.25	–1.04	–
B[b]	–	–	+1.30
BS[b]	–	–	+1.23

[a] Redox potentials *vs.* ferrocene/ferrocenium (Fc/Fc^+) in CH_2Cl_2 solutions, using Bu_4NPF_6 as supporting electrolyte at a scan rate of 100 mV s^{-1}. [b] Peak potentials measured in MeCN.

Time-resolved fluorescence and transient absorption spectroscopy

The competition between the PET process and the excimer relaxation pathway in **F2** and **F2S** was further investigated by time-resolved fluorescence and absorption techniques which allow us to access the singlet excited states of the folda-dimers. The fluorescence decay profiles were monitored at the monomer-like fluorescence band at 540 nm and the excimer band at 675 nm, respectively, which revealed clearly different behaviours (Fig. S3). When the monomer-type fluorescence band was directly probed, decay components with large amplitudes (64-66%) and time constants shorter than the instrumental response function (IRF) of our setup (~50 ps) were revealed in both **F2** and **F2S** irrespective of the solvent used, followed by the fluorescence lifetimes of the PBI monomer (2.0-3.0 ns).[17] We ascribe this fast fluorescence quenching to the PET process from the phenylethynyl-unit-containing backbones to the PBI acceptors. On the other hand, the decay profiles monitored at 675 nm were devoid of such rapid fluorescence quenching but rather consisted of the respective fluorescence lifetimes of the monomer (2.0-3.0 ns) and the forbidden excimer species (20.6 and 27.9 ns), indicating that PET pathway does not play a significant role in the deactivation of the excimer.

Fig. 6 shows the femtosecond transient absorption (TA) spectra of **F2** and **F2S** measured at a wide spectral range spanning the visible and near-infrared (NIR) region (450-1100 nm). The overall TA spectra were greatly dependent on the solvent-triggered PBI packing arrangement. Because it is well recognized that the formation of PBI radical anions gives rise to new sharp absorption bands at 713, 800 and 960 nm,[32,33] the spectral features of the positive excited-state absorption (ESA) bands serve as a direct measure of the efficiency of the PET process. In chloroform, where the open conformation prevails for both foldamers, an immediate rise of sharp ESA peaks at ~705 and 960 nm was observed upon photoexcitation to the singlet excited state of PBI, which corresponds to the ultrafast formation of PBI radical anions in the excited state as a result of photoinduced charge separation. The fitted time constants revealed charge separation times of 1.5 ps (**F2**) and 0.7 ps (**F2S**) followed by charge recombination times of 30-50 ps (Fig. S4). No nanosecond-order time components comparable to the singlet excited lifetimes of either a monomer or an excimer were observed at any probe wavelength, indicative of an efficient exciton quenching process *via* an ultrafast PET channel in the open random conformation.

On the contrary, the folded conformations of **F2** and **F2S** exhibited much broader ESA signals, in particular nearly structureless NIR bands, indicating that the PET process is largely suppressed in the stacked arrangement of the foldamers due to a much more efficient trapping to the energetically lower-lying excimer state aided by the enhanced contact between the two chromophores by π–π-stacking. The decay profiles did not show any fast time component which could be ascribed to the charge transfer process; rather, the transient species remained constant with nearly no decay in their population throughout the entire time window of our measurement, corroborating the extremely long excimer state lifetime. Notably, the ESA band of **F2S** at ~700 nm showed gradual red-shift and more pronounced broadening towards a plateau-like structure within 3 ns, which was not observed in **F2**. Combined with our findings in the steady-state fluorescence spectra where **F2S** showed a much more prominent excimer fluorescence band in THF, we conjecture that the excited-state relaxation pathway of **F2S** is almost exclusively governed by excimer trapping, and that the spectral shifts observed in the ESA bands can be ascribed to the structural rearrangement of the initially formed excimer species to the energetically

most favourable low-energy state, as has been reported by several theoretical and, spectroscopic reports on helically displaced self-assembled PBI aggregates.[34-36]

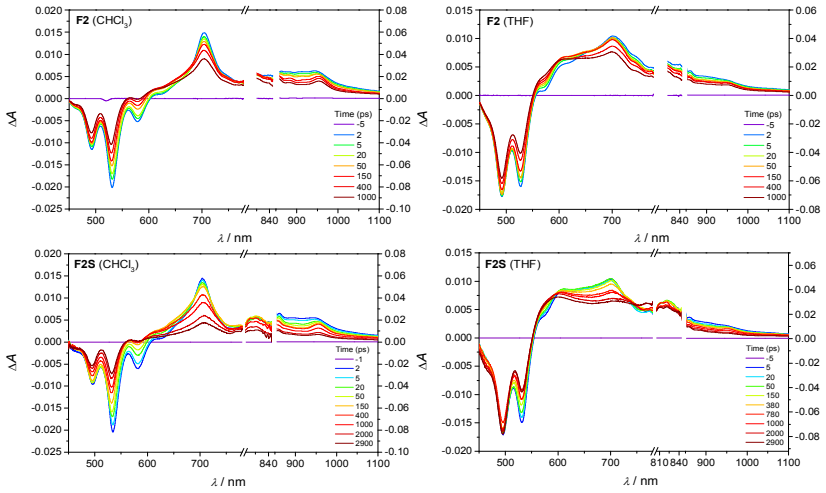

Fig. 6 Vis/NIR femtosecond-transient absorption spectra of **F2** (top) and **F2S** (bottom) in $CHCl_3$ (left) and THF (right). The pump wavelength employed was 530 nm for all measurements.

Discussion

Solvent-dependent folding and photophysical processes

Our spectroscopic results revealed equilibria between open and stacked conformations for both PBI dimers **F2** and **F2S**. Due to the ultrafast light-induced electronic excitation process, UV/Vis absorption spectra provide the best insight into the preferential populations of these conformations for the ground state molecules in solution. From these data we can conclude that both molecules prevail in more open conformations in chloroform and in more stacked conformations in THF, and that the equilibrium is more shifted towards the latter for folda-dimer **F2S**. This solvent effect can be rationalized by our earlier studies on the self-assembly of PBIs in which we could show that the binding constants between these dyes are lowest in chloroform and other chlorinated solvents due to their pronounced polarizability (largest refractive indices, leading to the highest dispersion interactions with PBI π-scaffolds).[37]

In contrast to the UV/Vis absorption spectra, fluorescence spectra are influenced by relaxation processes that occur within the lifetime of the excited molecules. Because different conformations may have very different fluorescence quantum yields, we further have to take into account that even minor species may govern the observed fluorescence spectra. This is clearly the case for both folda-dimers **F2** and **F2S** which still show emission spectra with typical vibronic progressions observed for a PBI monomer even in THF. Accordingly, the two higher-energy fluorescence bands at 533 and 575 nm are attributable to non-stacked conformations although the majority of the PBI dyes reside in THF in co-facially stacked state according to our UV/Vis studies as well as previous NMR analysis[17] for **F2**. Emissions from the folded molecules are nevertheless detectable as well in the form of red-shifted excimer emission bands at around 615 nm which are of weaker intensity because of

their more forbidden character.

The reduced fluorescence quantum yields in chloroform (despite the lower population of π-stacked folded conformations in this solvent) suggest the presence of other non-radiative deactivation pathways that are normally not observed for this class of dyes (see data in Table 1 for monomer **M1** which exhibit fluorescence quantum yields close to unity in both solvents). In particular, for **F2S**, fluorescence quantum yields of 18% were measured in both THF and chloroform, although in the former solvent emission mainly originates from the excimer state, whilst for the latter almost all fluorescence can be attributed to non-relaxed monomer-like PBIs. By means of transient absorption spectroscopy we were able to assign the competing quenching pathway to a PET process from the electron-rich phenylethynyl-unit-containing backbones of **F2** and **F2S** to the electron-poor PBI by unambiguous detection of the spectral features of PBI radical anions.[38] Accordingly, the major fluorescence quenching pathway for the more random open conformation in chloroform is a PET process whilst the major fluorescence quenching pathway for the stacked conformation in THF is the relaxation into the excimer state. Because the permittivity of the solvent chloroform (ε_r = 4.81) is smaller than that of THF (ε_r = 7.58), this pathway selectivity is not likely to arise from solvent stabilization of the charge separated state[39,40] but rather due to differences in the conformational preferences.

Implications for organic photovoltaics

In the following discussion we now try to relate the obtained insights onto the photophysical processes in excited PBI foldamers to those in bulk heterojunction solar cells composed of structurally related composites of electron-donating conjugated polymers and electron-poor PBIs (Fig. 7).[21,22,41-44] For these solar cells we can assume the following processes taking place: (1) absorption of sun light by PBI dyes or their aggregates, (2) ultrafast relaxation to the lowest Frenkel exciton state within less than 1 ps,[34] (3) exciton transport within PBI acceptor domains to the interface with the conjugated polymer donor material where (4) first charge transfer states are populated,[5] which subsequently may lead to the creation of a fully charge separated state (CS) with electrons and holes migrating through the donor (red shaded) and acceptor (blue shaded) phases towards the electrodes. It has been well considered that there are severe limitations to the transport of excitons in organic materials,[45] and due to the typically found exciton diffusion lengths of around 10 nm,[46] much effort has been devoted to accomplishing domains of this size in BHJ OSCs. However, it is difficult to get insight into the specific processes which compete with exciton migration and accordingly most studies assume trapping by disorder, grain boundaries, intermixed charge transfer complexes with some donor molecules, *etc.*

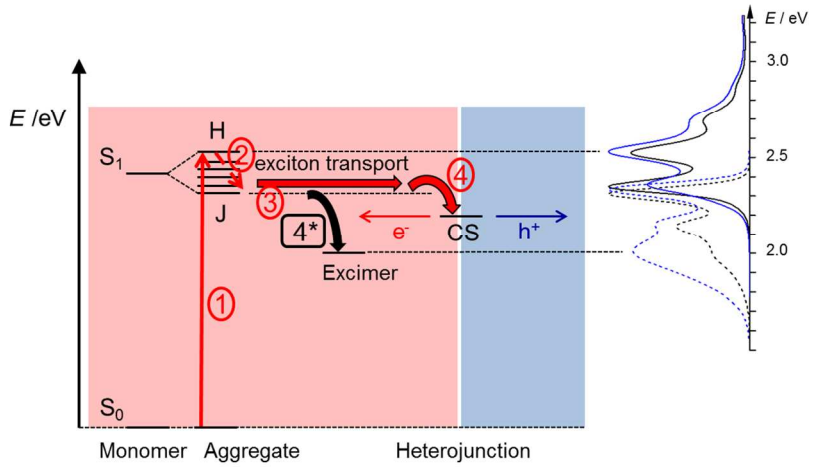

Fig. 7 Schematic energy state diagram describing light absorption by a PBI H-aggregate (1), exciton relaxation (2) to the lowest energy Frenkel exciton state (J-state), exciton migration to the heterojunction interface (3) and formation of a charge separated state (4) with subsequent migration of electrons and holes through the donor (red shaded) and acceptor (blue shaded) phases towards the electrodes. The absorption and emission spectra of folda-dimer **F2S** in THF (blue) and chloroform (black) are shown on the right side and related by dashed lines to the energy levels of the upper excitonic H-state and the excimer state in the schematic diagram on the left. Relaxation into the latter (4*) as a competitive pathway to exciton transport is illustrated as well.

Already a couple of years ago we and others have suggested that a major reason for the often poor performance of PBI-based solar cells compared to those based on fullerenes is the preference of PBI units for stacking into H-type aggregateswhose photoexcited states relax into excimer trap states.[47,48] Recently, time-resolved spectroscopy[36] and quantum dynamical studies[49] gave insight that within such H-aggregated PBIs, trapping to excimer states can indeed be quite fast, *i.e.* occurs in less than 50 ps. In the given study, however, we could take a step further and indeed elucidate the competing processes of desired charge separation (step 4) and undesired excimer formation (step 4*) within PBI foldamer heterojunction model systems **F2** and **F2S**. Indeed, based on our transient absorption data we can conclude that the excimer state (in THF) is obviously too low in energy to enable PET which could, however, be observed for the unfolded molecules (in chloroform). Accordingly, it is worth to have a closer look onto the energetics of the PET process by a Rehm-Weller analysis.

Driving force for PET by Rehm-Weller analysis

The Rehm-Weller analysis[50,51,52] based on equation (1) has been widely applied to estimate the thermodynamic driving force in molecular dyads and to figure out if PET processes occur in the Marcus normal or inverted region.[9,11,12,53] Accordingly, to approximate the driving force $\Delta G°$ for the respective PET processes, Rehm-Weller analyses were carried out with the available oxidation potentials E_{ox} for the two phenylene ethynylene backbones **B** and **BS** and the first reduction potentials E_{red} for PBI monomers and foldamers.

$$\Delta G° = e[E_{ox}(\mathrm{Don}) - E_{red}(\mathrm{Acc})] - E_{00} - \frac{e^2}{4\pi\varepsilon_0\varepsilon_S r} - \frac{e^2}{8\pi\varepsilon_0}\left(\frac{1}{r^+} + \frac{1}{r^-}\right)\left(\frac{1}{\varepsilon_{ref}} - \frac{1}{\varepsilon_S}\right) \qquad (1)$$

To carry out the Rehm-Weller analysis, in addition to the redox potentials (E_{ox}, E_{red}) of the electron donor and acceptor units, information on the intersection point (E_{00}) of the absorption and emission spectra of photoexcited component **M1** and the distance (r) between the centers of the donor and acceptor moieties as well as the dielectric constant of the solvent are required. Fortunately, the E_{00} values are almost not influenced by the utilized solvents and backbones of this study and also the polarity of the utilized solvents are in a similar range (although the permittivity of 4.81 for chloroform appears to be somewhat lower than those of 7.58 for THF and 8.93 for dichloromethane, the higher polarizability of the former creates a similar microscopic polarity) and therefore eq. (1) may be simplified by removing the solvent related term ($\varepsilon_{ref} = \varepsilon_S = 8.93$). Distances between centers of the donor and acceptor moieties were calculated based on geometry optimized structures obtained from calculations with the semi-empirical method PM6-DH2 which includes dispersion corrections (Fig. S14, S16 and Table S1). Due to the presence of folded and unfolded conformations two distances are given for both **F2** and **F2S** structures, which are, however, very similar, i.e. 10.6 Å for the folded and 12.5 Å for the unfolded states. Taking these values into eq. (1) shows that the impact of this distance variation is indeed minor (0.02-0.03 eV) and therefore we decided to use the smaller distance of 10.6 Å for the final analysis.

With a PBI reduction potential of –1.04 V (Table 2), oxidation potentials of +1.30 V (**B**) and +1.23 V (**BS**), an intersection point at 529 nm (2.35 eV), and donor-acceptor distances of 10.6 Å for **F2** and **F2S** the driving forces were estimated to be –0.22 eV for **F2S** and –0.15 eV for **F2**. Therefore, PET should be a weakly exergonic process in accordance with the observed light excitation-induced formation of PBI radical anions in chloroform. Obviously, however, the driving force is not large enough anymore from the excimer state in THF despite of the fact that THF is the more polar and therefore better charge-stabilizing solvent. This important result might be rationalized by a lowering of the E_{00} value in eq. (1) due to the energetic relaxation of the excited state as illustrated in Fig. 7. Accordingly, we conclude that while the PET processes would be energetically feasible for the initially excited folded states of PBI folda-dimers **F2** and **F2S** (whose more compact structures should in fact lead to a higher exothermicity compared to the expanded structures, see Table S1), the relaxation into the excimer state is the favoured exciton relaxation channel for the folded conformation. This result is now of critical relevance for OSCs based on PBI-containing acceptor components where excitons have to migrate over tens of molecules until they reach the heterojunction interface where the PET process takes place. In such a situation the PET process is obviously greatly disfavoured and relaxation processes within the light harvesting PBI manifold into excimer states thus have to be strictly suppressed by a molecular design that disfavours excimer formation. Indeed for those PBI dyes that afforded decent performance in BHJ OSCs with various conducting polymers[21,22,41-44] we can assume that different packing arrangements are present and/or that relaxation into excimers is prohibited by sterical means, which is in contrast to the easiness for this relaxation pathway observed in the more common rotationally stacked H-aggregated PBIs.

Conclusions

The electronic and structural factors that govern photoinduced electron transfer

(PET) processes have been of interest since several decades.[9-12] In this contribution we have elucidated how a transition from a more open conformation of a conjugated oligomer electron donor with appended non-interacting perylene bisimide (PBI) acceptor dyes to a conformation with π-stacked PBI acceptor dyes influences the photophysical behaviour of the donor-acceptor dyad system. Our study shows that for a situation that is quite related to the situation in heterojunction organic solar cells, *i.e.* low thermodynamic driving force for charge separation, an initially very efficient PET process for non-aggregated molecules (open conformation) may be completely suppressed upon dye aggregation due to a now thermodynamically favoured and kinetically fast relaxation channel into excimer trap states. Such relaxation paths are very fast for π-stacked PBI dyes which exhibit strongly coupled π-scaffolds and require only slight structural adjustments to enter deep traps on the excited state potential energy surface.[54] We assume that such relaxation pathways are of relevance for other flat π-systems as well and therefore should be considered in the research directed towards the replacement of globular fullerene acceptors by other organic semiconductor molecules in organic photovoltaics.

Acknowledgement

A. N.-K. thanks the Alexander von Humboldt foundation for a postdoctoral fellowship. The researchers from the Universität Würzburg acknowledge generous financial support from the Bavarian State Ministry of Science, Research, and the Arts for the Collaborative Research Network ‘‘Solar Technologies go Hybrid’’. The work at Yonsei University was financially supported by the Mid-career Researcher Program (2005-0093839) administered through the National Research Foundation of Korea (NRF) funded by the Ministry of Education, Science and Technology (MEST).

References

[a] *Universität Würzburg, Institut für Organische Chemie & Center for Nanosystems Chemistry, Am Hubland, 97074 Würzburg, Germany. Fax: +49-931-3184756; Tel: +49-931-3185340; E-mail: wuerthner@chemie.uni-wuerzburg.de*

[b] *Spectroscopy Laboratory for Functional π-Electronic Systems and Department of Chemistry, Yonsei University, Seoul 120-749, Korea. Fax: +82-2-2123-2434; Tel: +82-2-2123-2652; E-mail: dongho@yonsei.ac.kr*

† Electronic Supplementary Information (ESI) available: [details of any supplementary information available should be included here]. See DOI: 10.1039/b000000x/]

1 M. Schwoerer and H. C. Wolf, *Organic Molecular Solids*, Wiley-VCH, Weinheim, 2007.
2 F. Würthner and K. Meerholz, *Chem. Eur. J.,* 2010, **16**, 9366.
3 D. M. Bassani, L. Jonusauskaite, A. Lavie-Cambot, N. D. McClenaghan, J.-L. Pozzo, D. Ray and G. Vives, *Coord. Chem. Rev.,* 2010, **254**, 2429.
4 A. Dieckmann, H. Bässler and P. M. Borsenberger, *J. Chem. Phys.,* 1993, **99**, 8136.
5 J.-L. Brédas, J. E. Norton, J. Cornil and V. Coropceanu, *Acc. Chem. Res.,* 2009, **42**, 1691.
6 C. W. Tang, *Appl. Phys. Lett.,* 1986, **48**, 183.
7 Y. T. Fu, C. Risko and J.-L. Brédas, *Adv. Mater.,* 2013, **25**, 878.
8 B. P. Rand, D. Cheyns, K. Vasseur, N. C. Giebink, S. Mothy, Y. P. Yi, V. Coropceanu, D. Beljonne, J. Cornil and J.-L. Brédas, *Adv. Funct. Mater.,* 2012, **22**, 2987.
9 M. R. Wasielewski, *Chem. Rev.,* 1992, **92**, 6363.
10 J. L. Segura, N. Martín and D. M. Guldi, *Chem. Soc. Rev.,* 2005, **34**, 41.
11 A. C. Benniston and A. Harriman, *Chem. Soc. Rev.,* 2006, **35**, 169.
12 M. Natali, S. Campagna and F. Scandola, *Chem. Soc. Rev.,* 2014, **43**, 4005.

13 F. Würthner, Z. Chen, F. J. M. Hoeben, P. Osswald, C.-C. You, P. Jonkheijm, J. van Herrikhuyzen, A. P. H. J. Schenning, P. P. A. M. van der Schoot, E. W. Meijer, E. H. A. Beckers, S. C. J. Meskers and R. A. J. Janssen, *J. Am. Chem. Soc.,* 2004, **126**, 10611.
14 C. H. Huang, N. D. McClenaghan, A. Kuhn, J. W. Hofstraat and D. M. Bassani, *Org. Lett.,* 2005, **7**, 3409.
15 R. Bhosale, J. Misek, N. Sakai and S. Matile, *Chem. Soc. Rev.,* 2010, **39**, 138.
16 V. Dehm, M. Büchner, J. Seibt, V. Engel and F. Würthner, *Chem. Sci.,* 2011, **2**, 2094.
17 B. Fimmel, M. Son, Y. M. Sung, M. Grüne, B. Engels, D. Kim and F. Würthner, *Chem. Eur. J.*, 2015, **21**, 615.
18 M. Son, B. Fimmel, V. Dehm, F. Würthner and D. Kim, *ChemPhysChem,* 2015, **16**, 1757.
19 F. Würthner, *Chem. Commun.,* **2004**, 1564.
20 F. Würthner, C. R. Saha-Möller, B. Fimmel, P. Leowanawat, S. Ogi and D. Schmidt, *Chem Rev.,* **2015**, in press.
21 Y. Zhong, M. T. Trinh, R. Chen, W. Wang, P. P. Khlyabich, B. Kumar, Q. Xu, C.-Y. Nam, M. Y. Sfeir, C. Black, M. L. Steigerwald, Y.-L. Loo, S. Xiao, F. Ng, X. Y. Zhu and C. Nuckolls, *J. Am. Chem. Soc.,* 2014, **136**, 15215.
22 Y. Zang, C.-Z. Li, C.-C. Chueh, S. T. Williams, W. Jiang, Z.-H. Wang, J.-S. Yu and A. K. Y. Jen, *Adv. Mater.,* 2014, **26**, 5708.
23 A. J. Fry, in *Laboratory Techniques in Electroanalytical Chemistry*, ed. P. T. Kissinger, W. R. Heineman, Marcel Dekker Ltd, New York, 2nd edn., 1996, p. 481.
24 G. Seybold and G. Wagenblast, *Dyes Pigm.*, 1989, **11**, 303.
25 I. B. Berlman, *Handbook of Fluorescence Spectra of Aromatic Molecules*, Academic Press, New York, London, 2nd edn., 1971.
26 J. T. Fletcher and M. J. Therien, *J. Am. Chem. Soc.,* 2000, **122**, 12393.
27 J. Seibt, P. Marquetand, V. Engel, Z. Chen, V. Dehm and F. Würthner, *Chem. Phys.,* 2006, **328**, 354.
28 A. D. Shaller, W. Wang, A. Li, G. Moyna, J. J. Han, G. L. Helms and A. D. Q. Li, *Chem. Eur. J.,* 2011, **17**, 8350.
29 D. Veldman, S. C. J. Meskers and R. A. J. Janssen, *Adv. Funct. Mater.,* 2009, **19**, 1939.
30 A. Zitzler-Kunkel, M. Lenze, N. M. Kronenberg, A.-M. Krause, M. Stolte, K. Meerholz and F. Würthner, *Chem. Mater.,* 2014, **26**, 4856.
31 F. Schlosser, M. Moos, C. Lambert and F. Würthner, *Adv. Mater.* 2013, **25**, 410.
32 R. O. Marcon and S. Brochsztain, *J. Phys. Chem. A*, 2009, **113**, 1747.
33 M. Wolffs, N. Delsuc, D. Veldman, N. Vân Anh, R. M. Williams, S. C. J. Meskers, R. A. J. Janssen, I. Huc and A. P. H. J. Schenning, *J. Am. Chem. Soc.*, 2009, **131**, 4819.
34 A. Schubert, V. Settels, W. Liu, F. Würthner, C. Meier, R. F. Fink, S. Schindlbeck, S. Lochbrunner, B. Engels and V. Engel, *J. Phys. Chem. Lett*., 2013, **4**, 792.
35 E. A. Margulies, L. E. Shoer, S. W. Eaton and M. R. Wasielewski, *Phys. Chem. Chem. Phys*., 2014, **16**, 23735.
36 J. M. Lim, P. Kim, M-C. Yoon, J. Sung. V. Dehm, Z. Chen, F. Würthner and D. Kim, *Chem. Sci.,* 2013, **4**, 388.
37 Z. Chen, B. Fimmel and F. Würthner, *Org. Biomol. Chem.,* 2012, **10**, 5845.
38 J. Salbeck, H. Kunkely, H. Langhals, R. W. Saalfrank and J. Daub, *Chimia,* 1989, **43**, 6.
39 N. J. Turro, J. C. Scaiano and V. Ramamurthy, *Principles of Molecular Photochemistry: An Introduction*, University Science Books, Sausalito, CA, 2008.
40 V. May and O. Kühn, *Charge and Energy Transfer Dynamics in Molecular Systems*, Wiley-VCH, Berlin, 2001.
41 R. Shivanna, S. Shoaee, S. Dimitrov, S. K. Kandappa, S. Rajaram, J. Durrant and K. S. Narayan, *Energy Environ. Sci.,* 2014, **7**, 435.
42 T. Ye, R. Singh, H.-J. Butt, G. Floudas and P. E. Keivanidis, *ACS Appl. Mater. Interfaces,* 2013, **5**, 11844.
43 Y. Lin , Y. Wang , J. Wang , J. Hou , Y. Li , D. Zhu and X. Zhan, *Adv. Mater.*, 2014, **26**, 5137.
44 P. E. Hartnett, A. Timalsina, H. S. S. R. Matte, N. Zhou, X. Guo, W. Zhao, A. Facchetti, R. P. H. Chang, M. C. Hersam, M. R. Wasielewski and T. J. Marks, *J. Am. Chem. Soc.,* 2014, **136**, 16345.
45 G. D. Scholes and G. Rumbles, *Nat. Mater.,* 2006, **5**, 683.
46 J. D. A. Lin, O. V. Mikhnenko, J. Chen, Z. Masri, A. Ruseckas, A. Mikhailovsky, R. P. Raab, J. Liu, P. W. M. Blom, M. Antonietta Loi, C. J. García-Cervera, I. D. W. Samuel and T.-Q. Nguyen, *Mater. Horiz.,* 2014, **1**, 280.

47 Z. Chen, V. Stepanenko, V. Dehm, P. Prins, L. D. A. Siebbeles, J. Seibt, P. Marquetand, V. Engel and F. Würthner, *Chem. Eur. J.,* 2007, **13**, 436.
48 J. M. Giaimo, J. V. Lockard, L. E. Sinks, A. M. Scott, T. M. Wilson and M. R. Wasielewski, *J. Phys. Chem A*, 2008, **112**, 2322.
49 A. Schubert, M. Falge, M. Kess, V. Settels, S. Lochbrunner, W. T. Strunz, F. Würthner, B. Engels and V. Engel, *J. Phys. Chem. A,* 2014, **118**, 1408.
50 D. Rehm and A. Weller, *Ber. Bunsenges. Phys. Chem.,* 1969, **73**, 834.
51 D. Rehm and A. Weller, *Isr. J. Chem.*, 1970, **8**, 259.
52 A. Weller, *Z. Phys. Chem.*, 1982, **133**, 93.
53 R. M. Williams, *Introduction to Electron Transfer*, http://www.researchgate.net/publication/225188430_Introduction_to_Electron_Transfer, (accessed April 2015).
54 R. Fink, J. Seibt, V. Engel, M. Renz, M. Kaupp, S. Lochbrunner, H.-M. Zhao, J. Pfister, F. Würthner and B. Engels, *J. Am. Chem. Soc.*, 2008, **130**, 12858.